npj | science of food

Article

Published in partnership with Beijing Technology and Business University & International Union of Food Science and Technology

https://doi.org/10.1038/s41538-025-00691-6

Comprehensive transcriptomic and metabolomic analysis provides insight into transportation stress effects on fish muscle quality

Check for updates

Yujie Meng[1], Liangzi Zhang[2], Shikang Sang[1], Zenan Huang[1], Ru Liu[1], Juan You[1], Qilin Huang[1], Yong Long[3], Guili Song[3], Dan Jia[4] ✉ & Tao Yin[1] ✉

Transportation, a critical link in the aquaculture industry chain, triggers significant economic losses through stress-induced muscle quality deterioration in fish. This multi-omics study explored the mechanisms underlying transportation stress-induced quality deterioration of fish muscle. Transportation stress elevated cortisol, glucose, lactate dehydrogenase, and oxidative markers (SOD), alongside gill/liver tissue damage. Stress reduced muscle shear force, whiteness, and water-holding capacity, which were highly related to the disruption of muscular structure. Transcriptomics revealed dysregulation of AMPK, PI3K-Akt, FoxO, and MAPK pathways *via pfkfb*, *akt*, *gadd45*, *gabarap*, *jun*. Metabolomics highlighted TCA cycle disruption, altered fructose and mannose/pyruvate metabolism, and purine imbalance (e.g., D-mannose 6-phosphate, malate, IMP). Muscle quality parameters negatively correlated with oxidative stress (*gpx*) and apoptosis (*casp3/8/9*), but positively linked to DL-glutamine and D-fructose 6-phosphate. Results demonstrate that transportation stress impairs muscle quality *via* energy dysregulation, oxidative damage, and apoptosis, thus providing a theoretical basis to optimize aquaculture transport and reduce economic losses.

Transportation is a key link in the whole industry chain of fish. During this process, the fish will experience stress reactions due to changes in water quality, vibration, noise, crowding, etc., resulting in increased levels of cortisol (COR), glucose (GLU), and lactate dehydrogenase (LDH) in the blood[1]. At the same time, the content of the antioxidant enzymes like superoxide dismutase (SOD) and catalase (CAT) is altered[2], and the histological structure of gills, liver, and muscle may be deteriorated[1,3,4]. Strong stress can lead to fish death, resulting in significant economic losses.

Numerous studies have shown that although the fish are still alive after the stress of transit, the muscle quality will deteriorate[5–7]. Transportation conditions[6,8], fish species[9], and other factors influence stress effects on muscle quality in transit. In general, the cellular structure of fish muscle is disrupted after stress, and shear force, water holding capacity (WHC), and the content of umami amino acids decrease, while the content of lactic acid and bitter nucleotides increase[4,5,8]. It has been demonstrated that the effects of transport-related stress on muscle quality are related to physiological regulation in fish, such as oxidative stress, heat shock response, and inflammatory response, etc., involving gene expression and physiological metabolism[7]. However, the related studies are limited, and the deeper mechanisms need to be further investigated.

In the last few years, omics technology has advanced rapidly and been applied in the study of aquatic animal stress mechanism[6], food safety[10], and food processing[11], and has gradually been used to reveal how stress affects the muscle quality of aquatic animals. The transcriptome examines gene expression variations, whereas the metabolome focuses on changes in metabolites. Changes in gene expression may affect metabolite synthesis, and changes in certain metabolites may also affect gene expression. With joint analysis, alterations in gene expression and metabolites can be systematically correlated, leading to a comprehensive understanding of the mechanisms underlying changes in muscle quality. At present, the effects of ammonia nitrogen stress[12] and crowding stress[13] on the muscle quality of aquatic animals have been studied by combined omics. Transportation stress is a unique type of stress which involves numerous stressors such as crushing, noise, and ammonia nitrogen. The effect of this comprehensive

[1]College of Food Science and Technology, Huazhong Agricultural University, Wuhan, China. [2]Wuhan Business University, Wuhan, China. [3]State Key Laboratory of Breeding Biotechnology and Sustainable Aquaculture, Institute of Hydrobiology, Chinese Academy of Sciences, Wuhan, China. [4]College of Animal Science and Technology, Yunnan Agricultural University, Kunming, China. ✉e-mail: jiadan@ynau.edu.cn; yintao@mail.hzau.edu.cn

stress on fish muscle quality remains unexplored via joint omics. The combination of transcriptome and metabolome can reveal the molecular mechanisms responsible for alterations in fish muscle quality under stress.

This study aimed to investigate the effects of transportation stress on the muscle quality of silver carp. We postulated that the deterioration in silver carp muscle quality was associated with energy metabolism and oxidative stress. The specific objectives were to: (1) quantify physiological stress responses through cortisol, antioxidant enzymes, and expression of Caspase 3; (2) characterize muscle quality deterioration through alterations in nutritional composition, shear force, WHC, and color; (3) integrate transcriptomic and metabolomic data to elucidate the mechanisms underlying muscle quality deterioration.

Results

Changes of muscle quality of silver carp during transportation

To explore the changes of muscle quality of silver carp during transportation, we determined the muscle quality parameters (Table 1). The content of lipid and protein in muscle decreased as time extended, and the moisture and ash content did not change. With prolonged transportation, the pH value of silver carp muscle declined significantly, and the lactic acid (LD) content increased significantly. Muscle glycogen (GLY) content declined significantly when the transport time was prolonged from 3 to 12 h. Statistical analysis revealed a perfect negative trend between LD and GLY ($\rho = -1$, $p = 0.083$) and between LD and pH ($\rho = -1$, $p = 0.083$). The shear force decreased significantly. The value of L^* (lightness) and W (whiteness) showed a significantly decreasing trend. The a^* (redness) increased first and then decreased significantly. The WHC of the muscle showed a significant decline. ADP (5′-adenosine diphosphate) and AMP (5′-adenosine monophosphate) content decreased gradually ($p < 0.05$), and IMP (Inosine 5′-monophosphate) content increased ($p < 0.05$).

Changes of biochemical indexes of silver carp during transportation

Cortisol concentration in serum increased as time prolonged ($p < 0.05$) (Fig. 1A). GLU, LDH, urea, and creatinine levels in silver carp serum showed significant increases (Fig. 1B–E). SOD concentration in serum decreased significantly after 24 h of transport (Fig. 1F). SOD concentration in the liver was decreased after 12 h of transport, and increased after 24 h of transport ($p < 0.05$) (Fig. 1G). CAT concentrations in serum were the lowest at 12 h of transport and in the liver at 6 h, after which they both increased significantly ($p < 0.05$) (Fig. 1H, I). In the pre-transport period, the expression of *caspase-3* in both the gill and liver of silver carp did not change significantly. The expression increased significantly ($p < 0.05$) at 24 h (Fig. 1J, K).

Cellular structure of the gill, liver, and muscle

Gill, liver, and muscle tissues were damaged to varying degrees with the extension of transportation time (Fig. 2). At 3 h of transport, gill filaments had normal morphology, and most of them were not curved. At 24 h of transport, gill tissues had an abnormal structure, and most gill filaments were severely curved, stacked, tangled, and with their apical ends obviously enlarged. When transported for 3 h, the hepatocytes were structurally complete, tightly arranged, with clear nuclei and clear cell outlines. When transported for 24 h, the hepatocytes of the silver carp were structurally incomplete, loosely and haphazardly arranged, and with unclear cell outlines, with increased blood sinusoids and increased congestion. The blood sinusoids were enlarged and congested, and vacuoles appeared. At 3 h of transport, the muscle cells had little difference in area and were arranged regularly and uniformly. And at 24 h of transport, the cell areas and shapes were more uneven, and were arranged loosely and irregularly, and the gaps were enlarged.

Table 1 | Changes of muscle quality of silver carp during transportation

Transportation time	3 h	6 h	12 h	24 h
Proximate composition				
Moisture/%	80.45 ± 0.24^{a}	80.56 ± 0.23^{a}	80.80 ± 0.22^{a}	80.92 ± 0.15^{a}
Crude protein/%	18.68 ± 0.26^{a}	18.29 ± 0.02^{a}	17.85 ± 0.22^{b}	17.70 ± 0.26^{b}
Crude lipid/%	2.63 ± 0.29^{a}	2.56 ± 0.21^{a}	2.49 ± 0.28^{a}	2.08 ± 0.29^{a}
Ash/%	1.11 ± 0.04^{a}	1.13 ± 0.05^{a}	1.16 ± 0.08^{a}	1.19 ± 0.07^{a}
Lactic acid and muscle glycogen				
pH	7.11 ± 0.07^{a}	6.98 ± 0.08^{b}	6.78 ± 0.09^{c}	6.66 ± 0.10^{d}
LD /(mmol/g protein)	0.057 ± 0.004^{d}	0.082 ± 0.010^{c}	0.097 ± 0.007^{b}	0.131 ± 0.006^{a}
GLY/(mg/g)	0.77 ± 0.05^{a}	0.42 ± 0.03^{b}	0.36 ± 0.02^{c}	0.32 ± 0.03^{c}
Physical properties				
Shear force	412.40 ± 14.62^{a}	379.30 ± 12.35^{b}	359.10 ± 12.95^{c}	333.10 ± 11.99^{d}
L^*	48.11 ± 1.48^{a}	45.52 ± 0.79^{b}	43.56 ± 0.78^{c}	41.02 ± 0.56^{d}
a^*	-0.20 ± 0.13^{c}	0.37 ± 0.30^{ab}	0.47 ± 0.17^{a}	0.26 ± 0.24^{b}
b^*	-1.83 ± 0.85^{a}	-2.53 ± 0.72^{bc}	-2.11 ± 0.64^{ab}	-2.83 ± 0.41^{c}
W	48.07 ± 1.46^{a}	45.45 ± 0.79^{b}	43.52 ± 0.78^{c}	40.95 ± 0.57^{d}
WHC	81.00 ± 1.87^{a}	77.73 ± 1.32^{b}	74.20 ± 2.98^{c}	70.87 ± 2.17^{d}
ATP and its related metabolites				
ADP/(mg/100 g)	11.58 ± 0.87^{a}	9.68 ± 0.65^{b}	9.11 ± 0.16^{bc}	8.51 ± 0.53^{c}
AMP/(mg/100 g)	17.40 ± 0.80^{a}	15.16 ± 0.56^{b}	11.88 ± 0.38^{c}	9.46 ± 0.59^{d}
IMP/(mg/100 g)	265.10 ± 0.41^{d}	280.43 ± 1.04^{c}	291.67 ± 1.17^{b}	300.43 ± 1.46^{a}
HxR/(mg/100 g)	88.70 ± 1.01^{c}	111.09 ± 0.37^{a}	102.49 ± 0.73^{b}	85.36 ± 0.79^{d}
Hx/(mg/100 g)	9.59 ± 0.62^{bc}	9.20 ± 0.89^{c}	10.40 ± 0.98^{b}	11.52 ± 0.40^{a}
Total amount/(mg/100 g)	392.36 ± 3.61^{c}	425.55 ± 3.33^{a}	425.55 ± 3.32^{a}	415.27 ± 3.67^{b}

LD lactic acid, *GLY* glycogen, *WHC* water holding capacity, L^* lightness, a^* redness, b^* yellowness, *W* whiteness, *ADP* 5'-adenosine diphosphate, *AMP* 5'-adenosine monophosphate, *IMP* Inosine 5'-monophosphate, *HxR* inosine, *Hx* hypoxanthine. Different superscript lowercase letters in the same row indicate significant differences ($p < 0.05$).

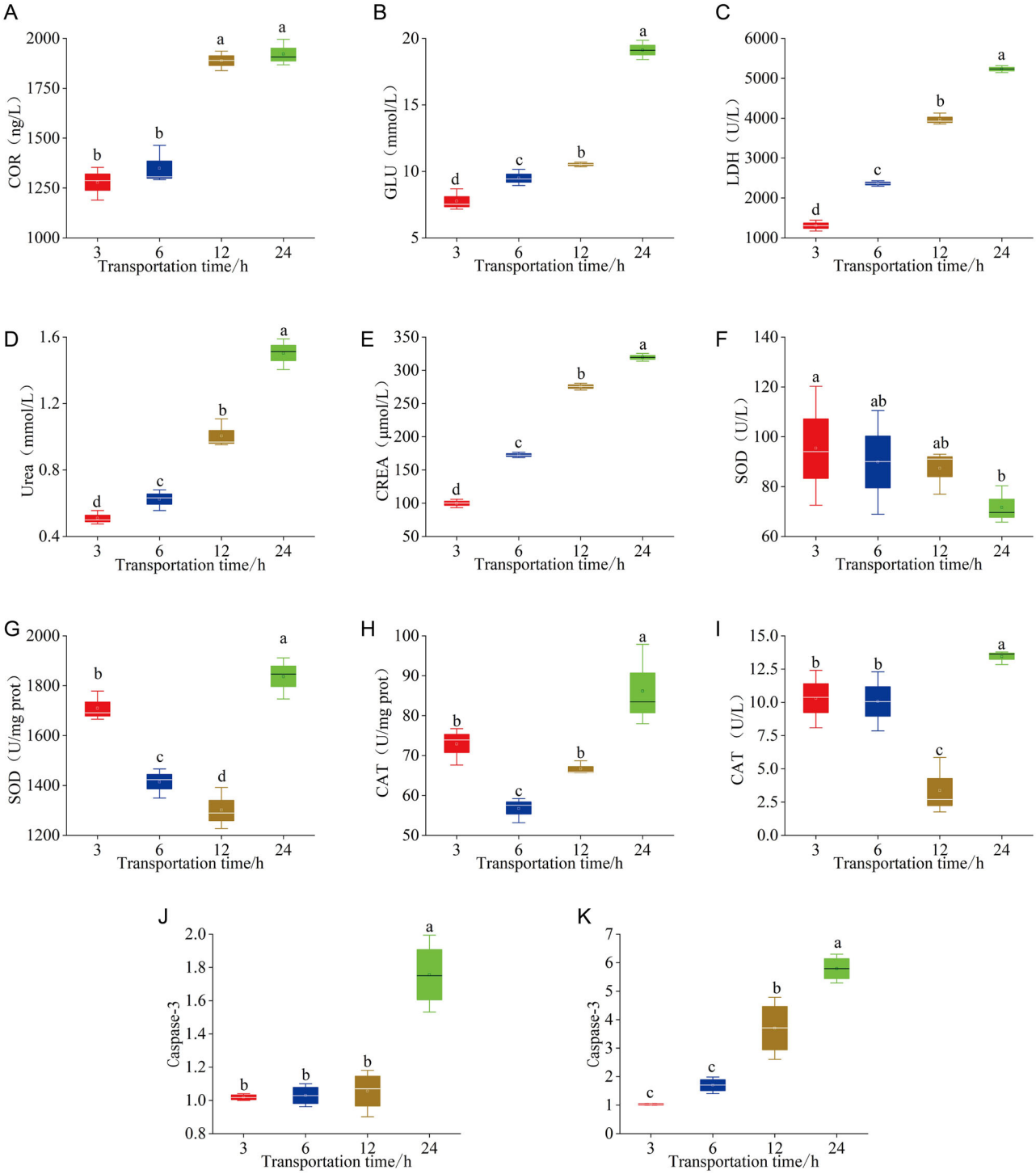

Fig. 1 | Changes on stress index of silver carp during transportation. A Serum cortisol. **B** Serum glucose. **C** Serum lactic dehydrogenase. **D** Serum urea. **E** Serum creatinine. **F** Superoxide dismutase of serum. **G** Superoxide dismutase of liver. **H** Catalase of serum. **I** Catalase of liver. **J** *Caspase 3* of the gill. **K** *Caspase 3* of the liver. COR cortisol, LDH lactic dehydrogenase, GLU glucose, CREA creatinine, SOD superoxide dismutase, CAT catalase.

Differentially expressed genes (DEGs) analysis and functional enrichment

The variability between T24 and T3 samples, or between T12 and T3 samples, was significant, while the variability between T6 and T3 samples was smaller (Fig. 3A). The number of DEGs gradually increased during transportation (Fig. 3B). There were 328 DEGs common to the three comparison groups (Table S2). The volcano plot analysis showed that the up-regulated DEGs were more than down-regulated DEGs for T6 vs T3, T12 vs T3, and T24 vs T3, respectively (Fig. 3C). To visually demonstrate the expression variations of DEGs between T6 vs T3, T12 vs T3, and T24 vs T3, hierarchical clustering heatmaps were generated (Fig. 3D). The results revealed significant differences among the different groups. The color gradient (blue to red) represents varying gene expression levels, with deep red signifying greater DEG abundance. The above findings indicated that the differences gradually increased as transportation duration lengthened.

For a deeper understanding of the biological processes involved in DEGs, GO enrichment analysis was performed. The study revealed that DEGs between T6 and T3 were predominantly associated with the

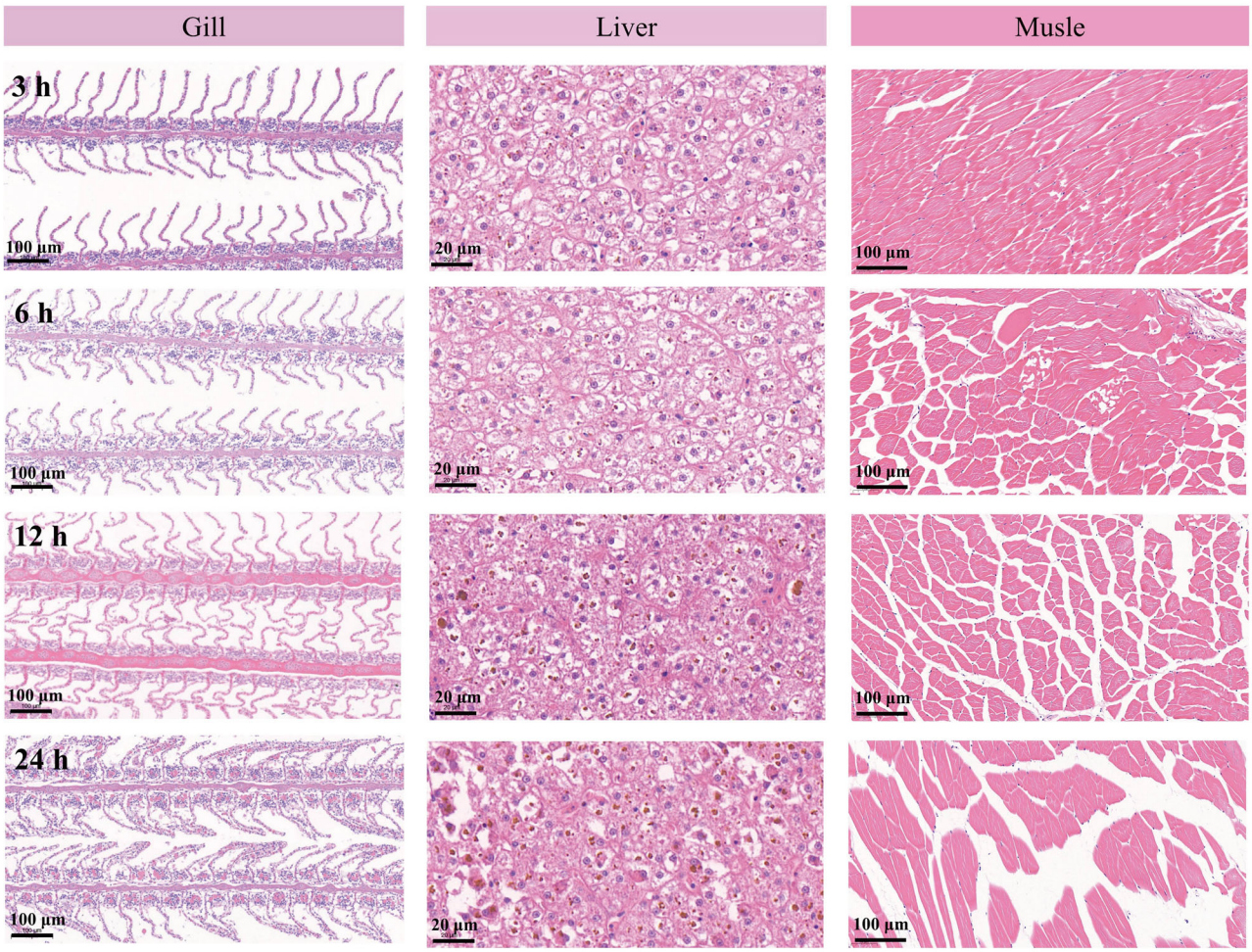

Fig. 2 | Changes on the histology of the gill, liver, and muscle tissues of silver carp during transportation.

regulation of cellular processes, regulation of biological processes, and biological regulation. DEGs between T12 and T3 were mainly enriched in the generation of precursor metabolites and energy, oxidation-reduction process, nucleoside monophosphate metabolic process, and purine nucleoside monophosphate metabolic process. T24 vs T3 DEGs were predominantly enriched in cellular process, response to wounding, MAPK cascade (Fig. 4A). Pancreatic secretion, cAMP signaling pathway, MAPK signaling pathway, citrate cycle (TCA cycle), and other pathways were among the enriched KEGG pathways for DEGs when transport time was extended from 3 to 6 h. Some DEGs of T12 vs T3 were significantly enriched in other types of o-glycan biosynthesis, AMPK signaling pathway, and other pathways. FoxO signaling pathway, protein digestion and absorption, PI3K-Akt signaling pathway, MAPK signaling pathway, Jak-STAT signaling pathway, and other pathways changed significantly from T3 to T24. Arginine and proline metabolism, the PPAR signaling pathway showed significant enrichment in T6 vs T3 and T12 vs T3. Autophagy, ether lipid metabolism, and mitophagy were significantly enriched in T12 vs T3h and T24 vs T3 (Fig. 4B). DEGs of silver carp under transportation stress primarily involve energy metabolism, oxidative stress, and apoptosis (Fig. S1A, Table S3).

The scale-free topological model fit was maximized by setting the soft threshold to 12 (Fig. 5A). Genes were divided into four modules (Fig. 5B). Correlations between gene modules and muscle quality indicators were analyzed. Meblue was significantly positively correlated with moisture, ash, LD, IMP, Hx and negatively correlated with crude protein, crude lipid, pH, GLY, ADP, AMP, shear force, L^*, b^* (yellowness), W, WHC (Fig. 5C). Fig. 5D showed the hub gene network in Meblue, in which *tbc1d1* (*TBC1 domain family member 1*) (ROI16019.1), *tepsin* (*AP-4 complex accessory subunit tepsin*) (ROI81943.1), *arfgap3* (*ADP-ribosylation factor GTPase-activating protein 3*) (ROL51222.1) may control muscle quality. For validation of the RNA-Seq data, qRT-PCR was used to assess the expression levels of 8 selected DEGs. The trends of these DEGs showed that the qRT-PCR and RNA-Seq data were basically consistent (Fig. 5E), supporting the reliability of the transcriptome dataset.

In this study, *hspb7* (*Heat shock protein beta-7*), *hspb1* (*Heat shock protein beta-1*), *hsp30* (*Heat shock protein 30*), *hspa13* (*Heat shock 70 kDa protein 13*), *hspa4* (*Heat shock 70 kDa protein 4*) were all up-regulated under stress (Table S3). The expression of oxidative stress-related gene *gpx* (*glutathione peroxidase*) and apoptosis-related genes *casp9* (*caspase 9*), *casp8* (*caspase 8*), *casp3* (*caspase 3*), *bad* (*Bcl2-associated agonist of cell death*), *tp53inp1*(*tumor protein p53 inducible nuclear protein 1*) were significantly altered by transportation stress (Table S3), suggesting that oxidative stress and apoptosis occurred in silver carp during transport.

Differential metabolites (DMs) analysis and functional enrichment

A total of 1319 metabolites were identified across both ion modes, including 775 in positive mode and 544 in negative mode. These metabolites contained lipids and lipid like molecules (24.11%), organic acids and derivatives (17.36%), organoheterocyclic compounds (15.09%), benzenoids (11.90%), organic oxygen compounds (8.04%), nucleosides, nucleotides and analogs (4.47%), etc. (Fig. 6A). Using univariate analysis, we examined metabolite variations in both ion modes, including unidentified compounds. As shown in Fig. 6B, the identified metabolites (Fold Change (FC) > 1.5 or FC < 0.67, p

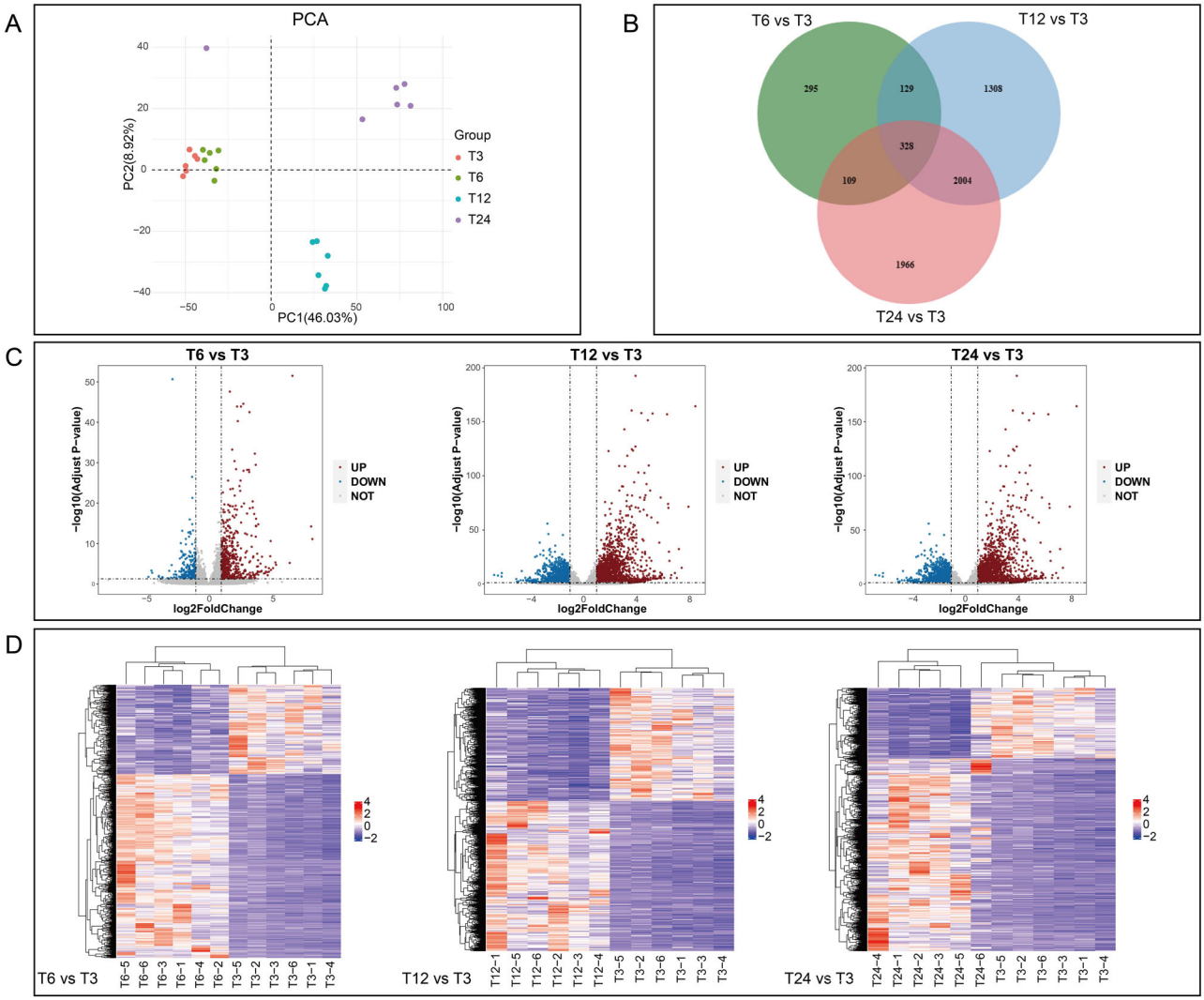

Fig. 3 | Screening of DEGs in the muscle of silver carp during transportation. **A** PCA analysis. **B** Venn diagrams. **C** Volcano plot. **D** Heat maps. T3, T6, T12, and T24 represent samples under transportation for 3, 6, 12, and 24 h.

value < 0.05) mainly included lipids and lipid-like molecules, nucleosides, and organic acids and derivatives. The OPLS-DA plot showed differences between different treatment groups (Fig. 6C), indicating that metabolites changed after transportation stress. It can be seen that the number of differential metabolites (DMs) (Variable Importance for the Projection (VIP) > 1, p value < 0.05) increases with the extension of transportation time (Fig. 6D). The name, retention time, molecular weight, and relative content ratios of DMs are shown in Table S4. To further investigate the potential metabolic pathways of DMs, annotation was conducted using the KEGG database (Fig. 6E). The metabolic pathways that differ between T6 and T3 samples were purine metabolism, oxidative phosphorylation, pentose and glucuronate interconversions, lysine degradation, and PI3K-Akt signaling pathway. Metabolic pathways that differ between T12 and T3 were citrate cycle (TCA cycle), pyruvate metabolism, AMPK signaling pathway, butanoate metabolism, glyoxylate and dicarboxylate metabolism. The metabolic pathways that differ between T24 and T3 were alanine, aspartate, and glutamate metabolism, galactose metabolism, fructose and mannose metabolism, ascorbate and aldarate metabolism, phenylalanine metabolism, amino sugar and nucleotide sugar metabolism. The FoxO signaling pathway was significantly enriched in T6 vs T3 and T12 vs T3 samples. Protein digestion and absorption, ferroptosis showed notable enrichment in T12 vs T3 and T24 vs T3 samples. Changes in relevant metabolic pathways and DMs were shown in Fig. S1B, Table S5.

Joint analysis of transcriptome and metabolome

DEGs and DMs were co-enriched into KEGG pathways. There were 35 KEGG pathways involved in DEGs and DMs of T6 vs T3 samples, 74 KEGG pathways involved in DEGs and DMs of T12 vs T3 samples, and 75 KEGG pathways involved in DEGs and DMs of T24 vs T3 samples (Fig. 7A). The significantly enriched pathways were shown in Fig. 7B. Next, Spearman correlation analysis was applied to assess DEG-DM relationships. The correlation coefficients and related p values are shown below: $|CC| > 0.5$ and $P < 0.05$ (T6 vs T3), $|CC| > 0.7$ and $P < 0.05$ (T12 vs T3), $|CC| > 0.7$ and $P < 0.05$ (T24 vs T3). Regulation of lipolysis in adipocytes, parathyroid hormone synthesis, secretion, and action were the most important metabolic pathways for silver carp to cope with stress when T6 samples were compared with T3 samples. When comparing T12 with T3 samples, the AMPK signaling pathway and gap junction were the most important metabolic pathways for silver carp to cope with stress. Protein digestion and absorption were the most important metabolic pathways for silver carp to cope with stress when T24 samples were compared with T3 samples. The DEGs and DMs involved were shown in Fig. 7C.

The protein expression of apoptosis-related genes

The expression levels of Bax increased significantly, while Bcl-2 expression levels first increased significantly before decreasing significantly. The Bax/

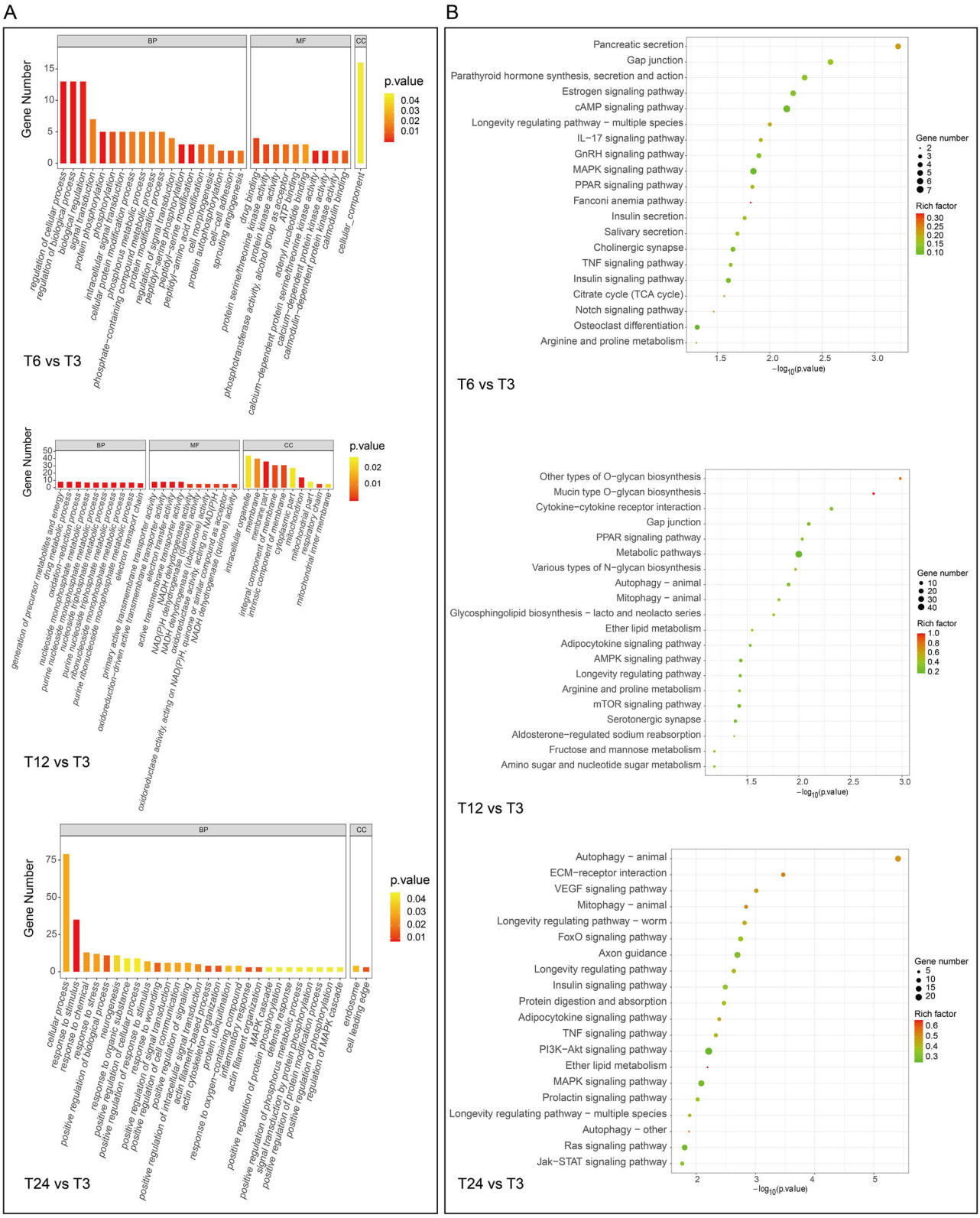

Fig. 4 | Functional analysis of DEGs in the muscle of silver carp during transportation. **A** The histogram of enriched GO terms. **B** The diagrams of KEGG pathways enrichment. T3, T6, T12, and T24 represent samples under transportation for 3, 6, 12, and 24 h.

Bcl-2 ratio increased significantly. The expression of Caspase3 and Caspase9 showed a trend of decreasing first and then increasing (Fig. 8). Above results further confirmed that apoptosis occurred in the muscle of silver carp during transportation.

Discussion

During transit, fish experience hunger and exposure to stressors like vibration and ammonia nitrogen. This triggers intensified struggling and elevated energy expenditure[14]. The decrease in lipid and protein (Table 1)

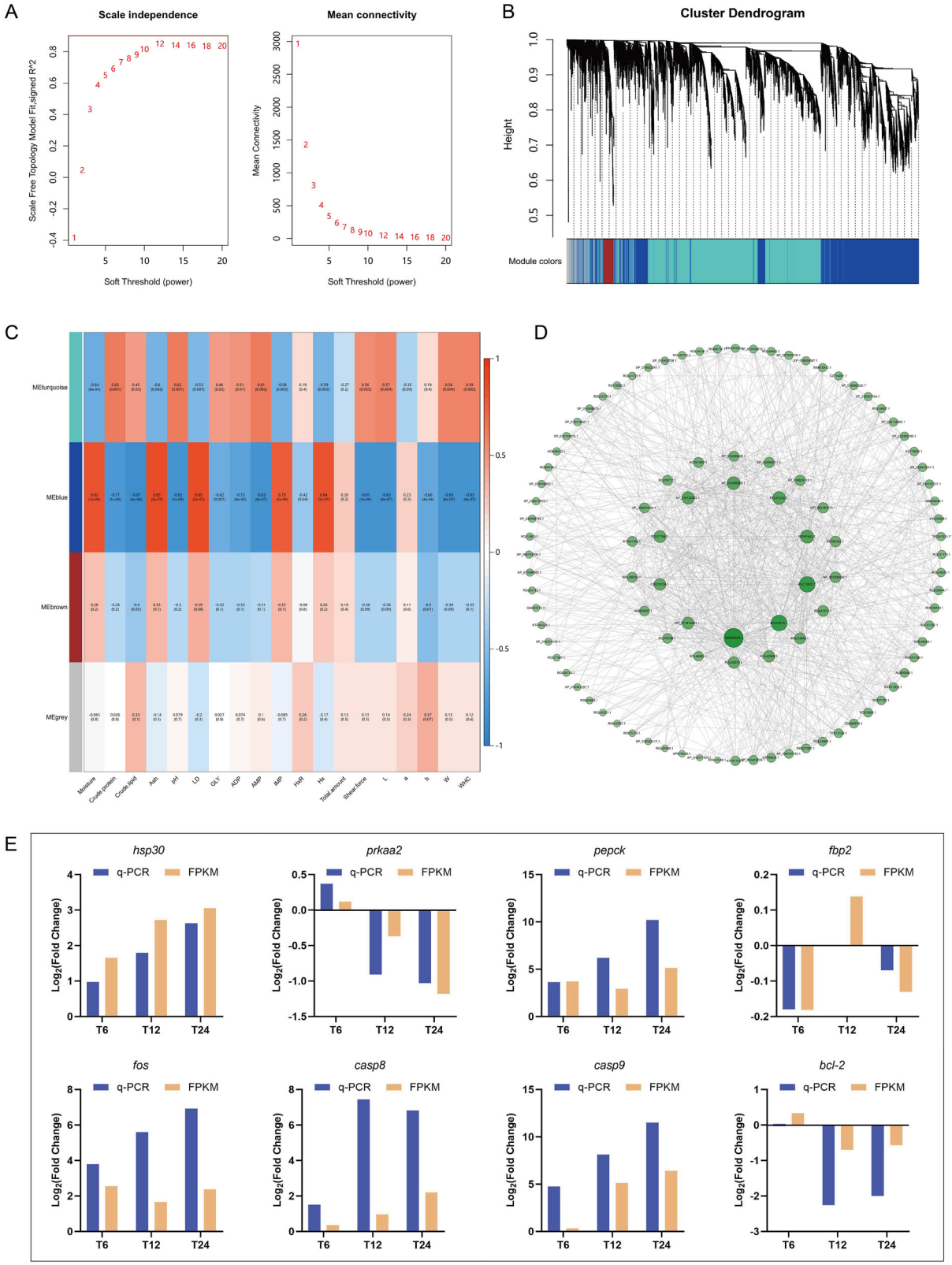

Fig. 5 | Coexpression network analysis of weighted genes (WGCNA) between the fish transported at different times with the muscle quality. A Soft threshold. **B** Clustering dendrograms of genes and modules division. **C** Heatmap of the correlation between gene module and the muscle quality. **D** Visualization of the top 100 genes in MEblue. **E** The relative expression level of DEGs by FPKM and qRT-PCR in the fish transported at different times.

content demonstrated that silver carp relied on lipid and protein as energy substrates[15]. As time was extended, GLY in muscle was rapidly degraded to produce energy for the life activities of fish[7]. The anaerobic glycolysis reaction was accelerated, generating a large amount of LD[16]. The accumulation of LD in muscle led to a decrease in muscle pH[17]. Hypothalamic-pituitary-interrenal (HPI) axis is activated during transportation of silver carp, which induces increased release of α-melanocyte-stimulating hormone[18]. α-melanocyte-stimulating hormone is the main

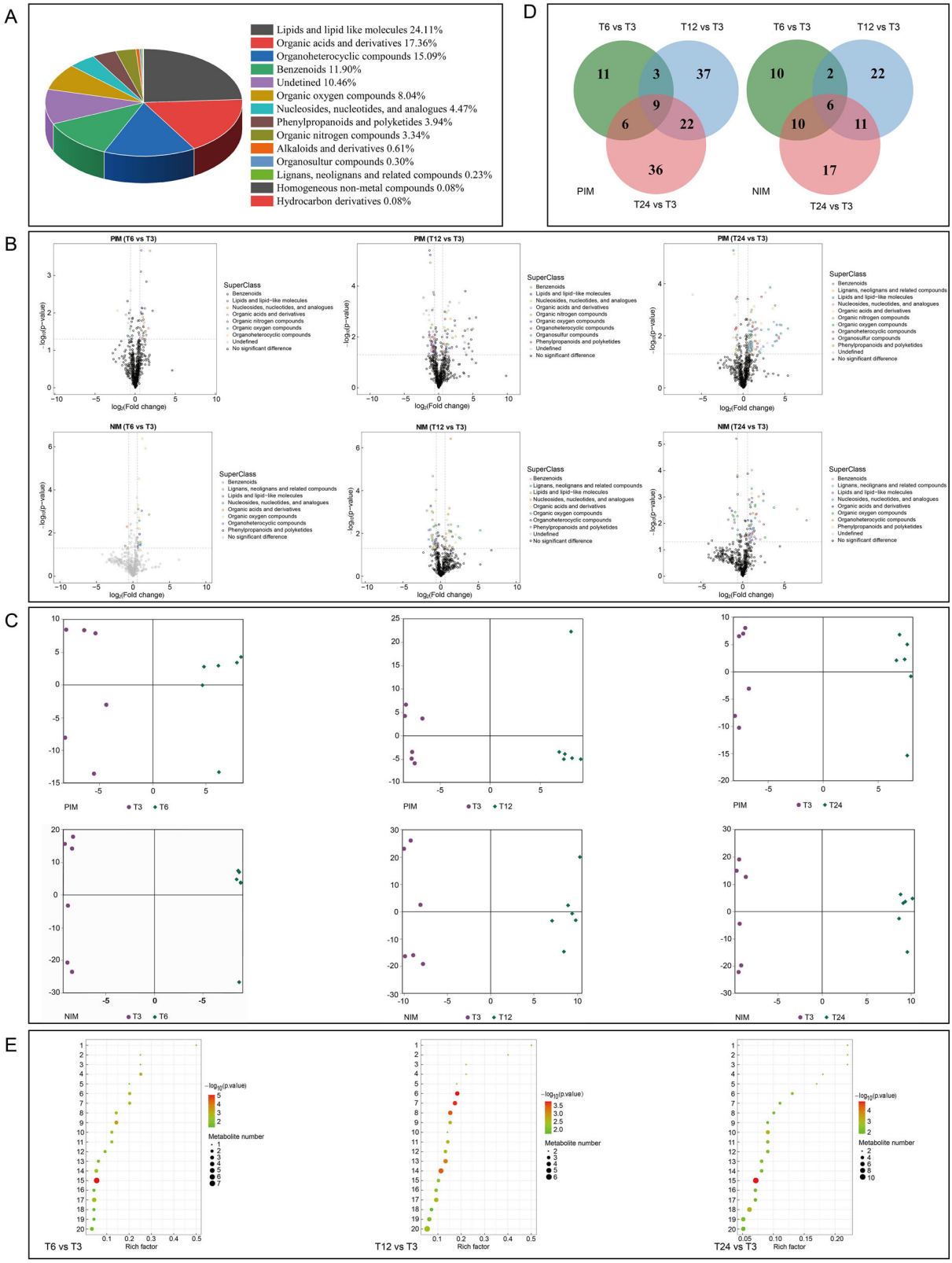

pigment control hormone in fish, which may be responsible for the reduction in L^*[7]. During the initial stage of transport, the muscle activity of fish increased, and the oxygen demand increased[1]. Myoglobin combined with oxygen to form oxymyoglobin. In the short term, the proportion of oxymyoglobin increased, showing a notable rise in a^*[8,19]. The decrease in a^* after 24 h may be due to the increased adaptation of the fish to the environment and the absence of violent struggles[20]. Changes in shear force are affected by a combination of factors, including myocyte structure, moisture, protein and lipid content, and protein denaturation[5,21]. The reduction in muscle shear force during transportation is likely attributed to muscle cell structure damage induced by apoptosis[22]. WHC characterizes the capability of muscle to absorb and hold water. The amount of net charge

Fig. 6 | Differential metabolites and their functional analysis in the muscle of silver carp during transportation. **A** The proportion of all metabolites. **B** Volcano plot of muscle metabolites. **C** OPLS-DA of muscle metabolites. **D** The Venn diagrams of differential metabolites. **E** The diagrams of KEGG pathways enrichment. T6 vs T3: 1. Cell cycle – yeast 2. PI3K−Akt signaling pathway 3. mTOR signaling pathway 4. Olfactory transduction 5. FoxO signaling pathway 6. cGMP−PKG signaling pathway 7. Parathyroid hormone synthesis, secretion, and action 8. Regulation of lipolysis in adipocytes 9. Aldosterone synthesis and secretion 10. Oxidative phosphorylation 11. Renin secretion 12. Thermogenesis 13. Taste transduction 14. Pentose and glucuronate interconversions 15. ABC transporters 16. Inositol phosphate metabolism 17. Purine metabolism 18. Ascorbate and aldarate metabolism 19. Lysine degradation 20. Amino sugar and nucleotide sugar metabolism. T12 vs T3: 1. Lysosome 2. FoxO signaling pathway 3. Long−term depression 4. Circadian entrainment 5. Gap junction 6. Taurine and hypotaurine metabolism 7. Thermogenesis 8. Glucagon signaling pathway 9. Citrate cycle (TCA cycle) 10. Platelet activation 11. AMPK signaling pathway 12. Carbon fixation in photosynthetic organisms 13. Pyruvate metabolism 14. Protein digestion and absorption 15. Ferroptosis 16. Taste transduction 17. Carbon fixation pathways in prokaryotes 18. Butanoate metabolism 19. Glyoxylate and dicarboxylate metabolism 20. Carbon metabolism. T24 vs T3: 1. Long−term depression 2. GABAergic synapse 3. Circadian entrainment 4. Gap junction 5. Synaptic vesicle cycle 6. Thermogenesis 7. Alanine, aspartate, and glutamate metabolism 8. Ferroptosis 9. Taste transduction 10. Fructose and mannose metabolism 11. Galactose metabolism 12. Protein digestion and absorption 13. Ascorbate and aldarate metabolism 14. Aminoacyl −tRNA biosynthesis 15. ABC transporters 16. Phosphotransferase system (PTS) 17. Phenylalanine metabolism 18. Amino sugar and nucleotide sugar metabolism 19. Carbon metabolism 20. Biosynthesis of amino acids. PIM stands for positive ion mode, and NIM stands for negative ion mode. T3, T6, T12, and T24 represent samples under transportation for 3, 6, 12, and 24 h.

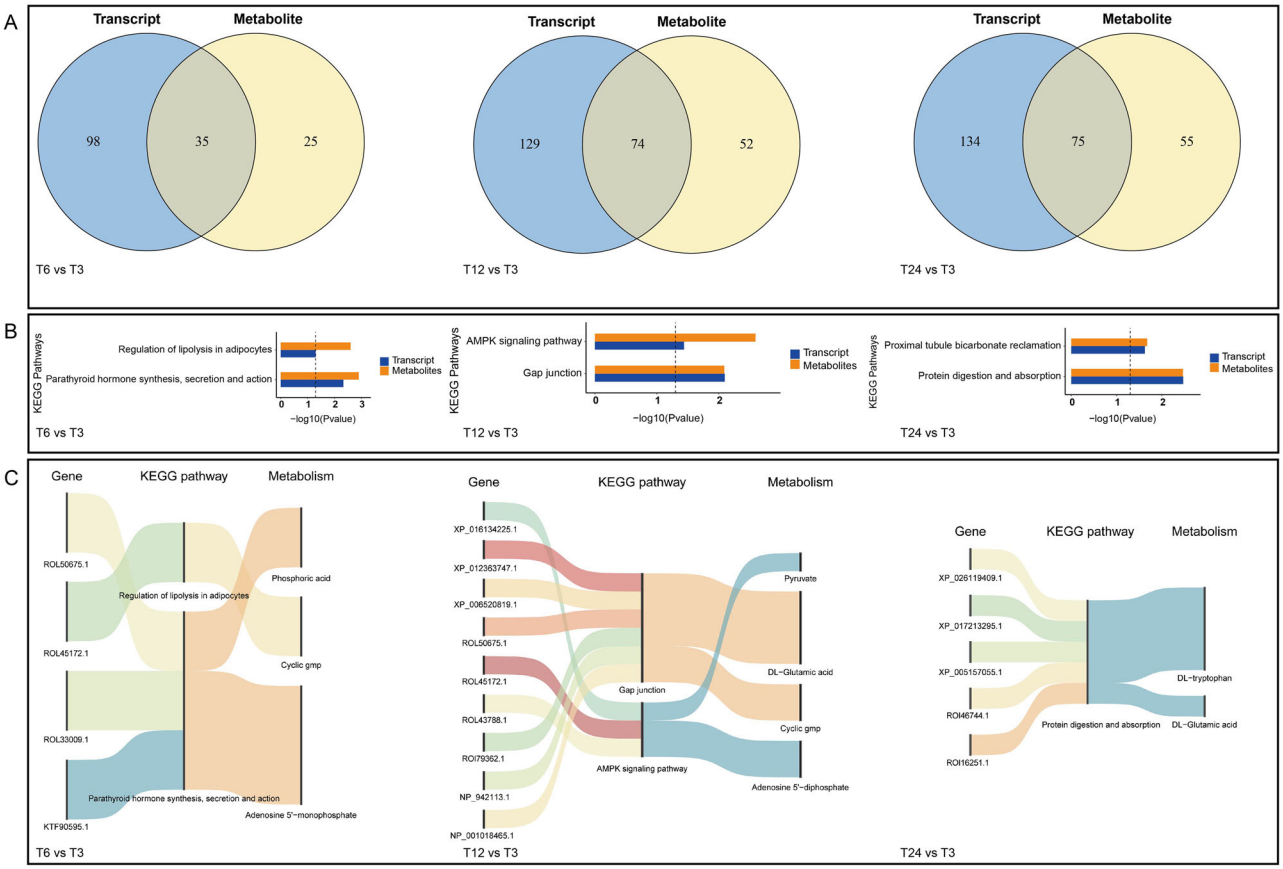

Fig. 7 | KEGG pathway of DEGs and DMs in the muscle of silver carp during transportation. **A** Venn diagrams of pathways involving DEGs and DMs. **B** KEGG enrichment histogram of DEGs and DMs. **C** Correlation network among DEGs and DMs. T3, T6, T12, and T24 represent samples under transportation for 3, 6, 12, and 24 h.

of myofilament affects the distance between myofilaments and ultimately affects the WHC of muscle[23]. pH can affect the WHC by affecting the net charge of muscle protein[24]. Muscle WHC is also related to cell structure. Muscle cell structure rupture led to tissue fluid loss and decreased muscle WHC[14]. Some of the ATP-related compounds have taste-producing properties, in which IMP can give umami to aquatic products, while HxR and Hx can make meat bitter[14]. Cao et al.[17] reported IMP and HxR content in Turbot (*Scophthalmus maximus*) muscle increased firstly and then decreased with the prolongation of time, and Hx content increased gradually, which aligned with the findings of this study.

Cortisol and blood glucose levels are common indicators for evaluating fish stress[25,26]. During transportation, a sharp increase in water ammonia and nitrite concentrations, along with constant stimulations such as collisions with the fish, activated the HPI axis and released cortisol[9,27]. When fish experience stress, energy consumption increases, inducing glycogen decomposition or gluconeogenesis, resulting in glucose entering the blood[28] and subsequently increasing blood glucose concentration (Fig. 1). The increase of LDH activity indicated that the anaerobic respiratory metabolic pathway of silver carp was enhanced[1]. The increase in serum urea content reflected the accumulation of protein metabolites[29]. A gradual increase in serum creatinine levels indicates possible damage to kidney function[25]. SOD and CAT are common indicators for quantitative studies of oxidative stress. Under normal conditions, the antioxidant system of fish maintains a dynamic balance. Stress exposure in fish leads to the generation of substantial reactive oxygen species (ROS), thereby influencing the activity of antioxidant enzymes[1]. The activities of SOD and CAT decreased during a short period of transportation (Fig. 1), which is in accordance with the findings reported by Wu et al.[6]. ROS is mainly produced by mitochondrial

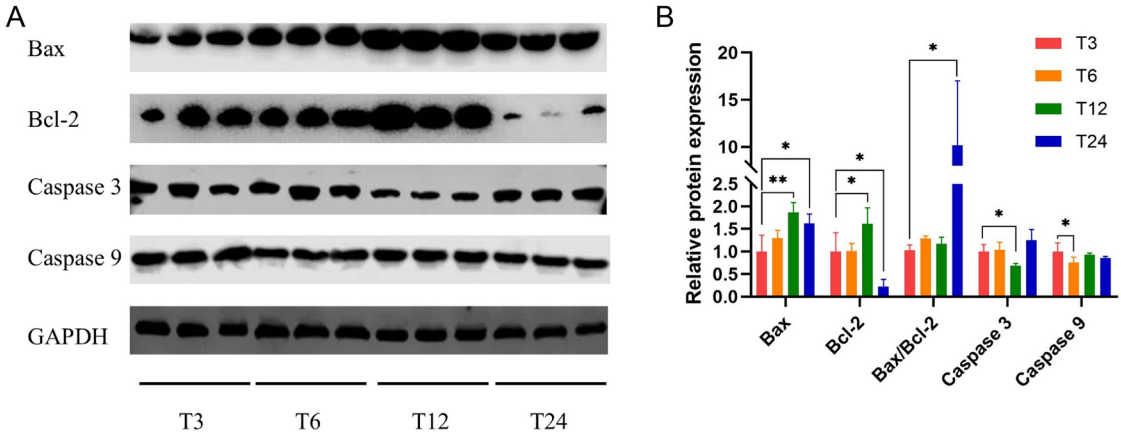

Fig. 8 | The protein expression of *caspase9*, *caspase3*, *bax*, and *bcl-2*. **A** The protein levels of *caspase9*, *caspase3*, *bax*, and *bcl-2*. **B** Western blot quantification data normalized to GAPDH (ImageJ analysis). $^{*}p < 0.05$, $^{**}p < 0.01$. T3, T6, T12, and T24 represent samples under transportation for 3, 6, 12, and 24 h.

electron leakage during aerobic respiration. ROS is a signal molecule that initiates a variety of physiological regulations in fish. In order to cooperate with the production of ROS, the activities of SOD and CAT were inhibited during the initial phase of stress exposure. Due to prolonged time and excessive ROS production, the activities of SOD and CAT increased to eliminate ROS, thereby preserving the redox equilibrium of fish[1]. The phenomenon of gill, liver, and muscle damage (Fig. 2) is similar to that observed by Peng et al.[4]. Oxidative stress oxidized myofibrillar proteins, thereby causing their fragmentation and ultimately disrupting the muscle tissue structural[30].

Citrate cycle (TCA cycle) is the ultimate common pathway for the oxidation of carbohydrates, proteins, and lipids[31,32]. Within the mitochondria, the TCA cycle generates energy during aerobic metabolism and is involved in many metabolic pathways in the cell[33]. Pyruvate is an important intermediate, which can be converted to acetyl-CoA by pyruvate metabolism and participates in the TCA cycle, which is essential for energy metabolism[34]. By catalyzing the transformation of oxaloacetate to phosphoenolpyruvate, phosphoenolpyruvate carboxykinase (PEPCK) establishes a metabolic link between the TCA cycle and the glycolysis pathways[35]. As the initial rate-limiting enzyme of the TCA cycle, 2-oxoglutarate dehydrogenase (OGDH) catalyzes the α-ketoglutarate to succinyl-CoA transformation, playing a pivotal role in glucose metabolism[36]. The up-regulated expression of *pfkfb* (*6-phosphofructo-2-kinase*) indicated an increase in glycolytic rate. Transportation stress activated the AMPK signaling pathway. AMPK signaling pathway can promote glucose uptake by muscle cells and regulate energy homeostasis[37,38]. Activation of the AMPK signaling pathway exacerbates muscle glycolytic flux under stress, leading to LD accumulation in the muscle[39]. The decrease in pH induced protein denaturation, which disrupted the tissue structure and impaired muscle WHC[40]. Increased expression of *pla2g4a* (*Cytosolic phospholipase A2*) causes phospholipid breakdown in cell membranes, altering permeability and releasing free fatty acids[41]. Up-regulation of *pla2g4a* expression indicated that Ether lipid metabolism was enhanced in stress. *pparα* can regulate free fatty acid transport and modulate muscle lipid content[42]. Purines serve as indispensable metabolites in all organisms and are implicated in diverse cellular processes, such as energy metabolism and cell signaling[43]. After sufficient breakdown of ATP, endogenous and exogenous proteases would destroy myofibrils and collagen fibers[44], and the tissue structure of fish would be destroyed.

Extracellular protein-regulated protein kinase (ERK), c-Jun N-terminal kinase (JNK), and p38 play key roles in the MAPK signaling pathway, and the activation of the MAPK signaling pathway promotes cell apoptosis[45]. Phosphorylation of ERK, JNK, and p38 induces the activation of activator protein-1 (AP1), followed by a cascade reaction and eventual apoptosis[46]. AP1 is an important transcriptional regulator assembled from members of the c-Jun and c-Fos protein families[47]. In this study, we found that *jun*, *fos*, and *jund* expression was up-regulated, indicating that transportation stress activated the MAPK signaling pathway, which in turn led to apoptosis in silver carp muscle cells. The PI3K-Akt signaling pathway serves as a key intermediary in cellular signal transduction, influencing cell survival and death[48]. In our study, the expression of *irs1b* (*Insulin receptor substrate 1-B*), *pik3cg* (*Phosphatidylinositol 4,5-bisphosphate 3-kinase catalytic subunit gamma isoform*), *akt* (*AKT serine/threonine kinase 2*), and *bcl2l1* (*Bcl-xl*) was up-regulated. *akt* is a *pik3cg*-regulated gene that mediates extracellular stress resistance[49]. Activated *akt* can exert anti-apoptotic effects by blocking the binding of *bad* (*Bcl2-associated agonist of cell death*) to *bcl2l1* to form a dimer, thereby increasing the free intracellular apoptosis suppressor *bcl2l1*[50]. DEGs enriched in the FoxO signaling pathway include *gadd45* (*growth arrest and DNA damage-inducible GADD45 alpha-like protein*) and *gabarap* (*gamma-aminobutyric acid receptor-associated protein*). Up-regulation of *gadd45* expression is a response to DNA damage or apoptosis[51]. *gabarap* expression is involved in autophagy and apoptosis[52]. In the Jak-STAT signaling pathway, *bcl2l1* was up-regulated and involved in anti-apoptotic response. Apoptosis contributed to the destruction of muscle fibers and the fragmentation of skeletal proteins, resulting in a decrease in shear force[30]. Apoptosis affects muscle cells through caspases-mediated proteolysis[53]. Increased expression of caspases leads to the disruption of Z-lines in myofibrils, and this structural damage subsequently reduces the shear force of fish muscle. Moreover, Caspase 9 and Caspase 3 degrade cytoskeletal proteins in muscle cells, which impairs cell-membrane adhesion and leads to water loss from the intercellular spaces, ultimately diminishing the water-holding capacity of the muscle[54].

The relationship between genes, metabolites, and WHC, shear force, and whiteness was shown in Fig. 9A. *tubb6* (*tubulin beta-6 chain*), γ-aminobutyric acid was negatively correlated with WHC, shear force, whiteness, and DL-glutamine, D-fructose 6-phosphate were positively correlated with WHC, shear force, whiteness. Fish muscle contains microtubules[55], a part of the cytoskeleton that maintains the structure of the cell[56]. Overexpression of *tubb6* disrupts the microtubule network[57], thereby disrupting the cytoskeleton. DL-glutamine can improve the antioxidant capacity of cells[58], thereby reducing muscle oxidative stress. There is a positive correlation between improved antioxidant capacity and muscle WHC[59]. The increase in DL-glutamine content promoted an elevation in muscle fiber density and a reduction in muscle fiber diameter. Notably, shear force exhibited a positive correlation with muscle fiber density and a negative one with fiber diameter, respectively[60]. γ-aminobutyric acid is an inhibitory neurotransmitter that can regulate the stress response by regulating the HPI axis activation[61]. The change of D-fructose 6-phosphate content can change the energy metabolism of cells[62]. The significant enrichment of carbohydrate metabolism-related pathways showed that the response of silver carp to transportation stress was highly correlated with carbohydrate metabolism. Silver carp was stimulated by vibration, starvation, and hypoxia during transport, the HPI

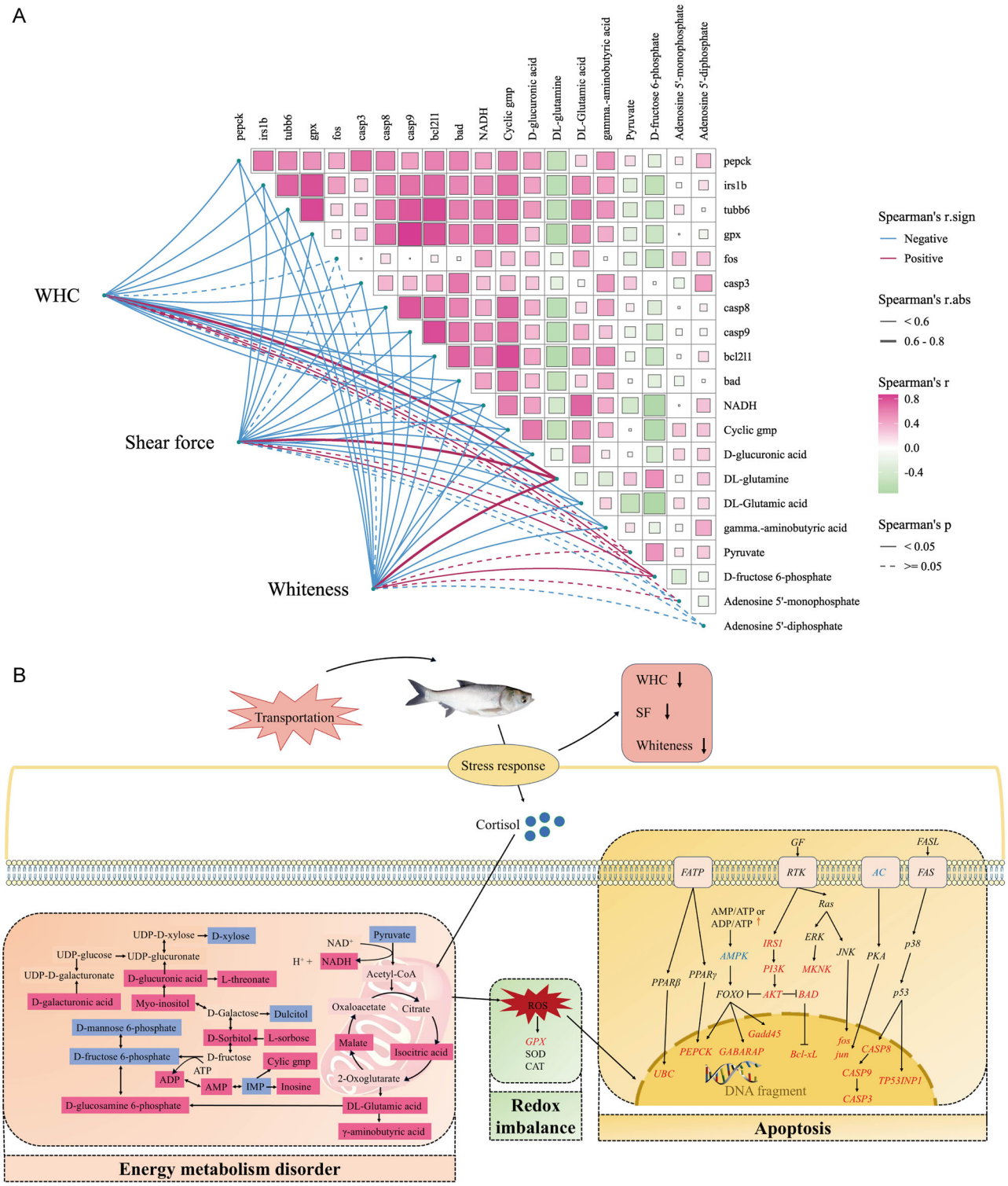

Fig. 9 | Schematic model illustrating the mechanism on transportation stress affecting the muscle quality of silver carp. A Correlation between muscle quality and DEGs, DMs. **B** Mechanisms of transportation stress on muscle quality of silver carp (*Hypophthalmichthys molitrix*). Metabolites in the red background box are up-regulated, and those in the blue background box are down-regulated. Altered genes were shown with red (up-regulated) and blue (down-regulated) marker names, respectively.

axis was activated, and the adrenal glands secreted cortisol. Cortisol induced mitochondrial dysfunction[63], leading to changes in metabolic pathways such as the TCA cycle, galactose metabolism, fructose and mannose metabolism, pyruvate metabolism, and purine metabolism. Maintaining internal homeostasis requires significant energy, making a steady energy supply essential for countering environmental disruptions[46]. Imbalance in energy metabolism causes an imbalance in intracellular homeostasis, leading to increased mitochondrial dysfunction[64]. Mitochondria produced ROS through the electron leakage of the electron transport chain[65]. Although fish scavenged ROS by expressing antioxidant enzymes, sustained and rapid ROS accumulation resulted in redox imbalance[66]. Under stress, ROS attacked DNA, activated the MAPK signaling pathway, the cAMP signaling

pathway, the PPAR signaling pathway, the PI3K-Akt signaling pathway, the FoxO signaling pathway, etc., induced the expression of pro-apoptotic genes *casp9*, *casp8*, *casp3*, *bad*, *tp53inp1*, and promoted apoptosis. Consequently, apoptosis resulted in reduced muscle shear force, WHC, and whiteness (Fig. 9B).

The study showed that transportation stress resulted in the destruction of muscle cell structure, the decrease of shear force, WHC, and whiteness, and the increase of unpleasant flavor substances (LD, Hx). The mechanism of muscle quality deterioration was related to the energy metabolism disorder, redox system imbalance, and apoptosis of silver carp induced by stress. These physiological changes mainly involved signaling pathways such as the MAPK signaling pathway, the FoxO signaling pathway, metabolic pathways such as the TCA cycle, Purine Metabolism, genes such as *pfkfb*, *jun*, *fos*, *gadd45*, *gpx*, metabolites such as Malate, Pyruvate, D-fructose 6-phosphate, IMP. The study provided new insights into the molecular mechanism of muscle quality changed in silver carp under transportation stress. However, the varying stress responses to transportation among different fish species may lead to distinct changes in muscle quality, highlighting the need for comparative studies across species. Future research should further validate the involved pathways through methods such as gene knockout model fish or the application of pathway blockers or activators.

Methods

Materials and experimental design

Silver carp were harvested from a fish pond of Dushan Town, Ezhou City, Hubei Province, China. The average weight of these fish is 1100 ± 100 g, the average length is 42.5 ± 3.3 cm, and the average width is 12.3 ± 1.4 cm.

All animal experimental procedures had been approved by the Animal Care and Use Committee of Huazhong Agricultural University (Approval No. HZAUFI-2023-0027). Transportation method referenced Xiang et al.[67]. Following harvest from the pond, silver carps underwent randomized allocation into four experimental cohorts ($n = 9$ per group) and were promptly transferred to aerated polyethylene boxes (54.5 × 37.0 × 34.5 cm). Water was dispensed into boxes at a 2:1 volume-to-weight ratio relative to fish weight, with ice pack supplementation maintaining a hypothermic environment. The pH of water was 6.58, the salinity was 199 mg/L, and the concentration of ammonia nitrogen was 0.21 mg/L. The transportation of fish to the laboratory was completed within 2 h. After the boxes got to the laboratory, they were placed on a simulated transportation platform (DK-5024, Xing suo Intelligent Equipment Co., Ltd., Xiamen, China) and continued to be transported at 120 rpm/min for 24 h. During transport, water temperature was sustained around 10 °C, and oxygen was filled with an oxygen cylinder to maintain the dissolved oxygen level at approximately 7 mg/L.

After transport times of 3, 6, 12, and 24 h (T3, T6, T12, and T24), respectively, six fish were removed from the box and killed by rapid striking with the back of a knife. Blood was immediately taken from the fish's tail, and the liver, gills, and dorsal muscles were dissected for analysis.

Measurement of the basic nutritional composition of muscle

To measure the moisture content, the sample was dried in an oven (Jinghong Experimental Equipment Co., Ltd., Shanghai, China) (105 °C) until its weight remained constant. Following acid digestion, the Kjeldahl method was employed to determine the protein content of the samples. Soxhlet extraction was utilized to measure the lipid content. The content of ash was determined by burning the sample in a muffle furnace (4-10 Kanglu Instrument and Equipment Co., Ltd., Shanghai, China) (550 ± 25°C) for 4 h. Three muscle samples were analyzed per treatment group.

Measurement of muscle pH, lactic acid (LD) content, and glycogen (GLY) content

A pH-meter (Testo 205 Dettol Instruments International Trading Co., Ltd., Shanghai, China) was employed to measure the muscle pH. The contents of muscle GLY and LD were determined with commercial kits (Nanjing Jiancheng Bioengineering Institute, Nanjing, China). Twenty muscle samples were taken from each treatment group to measure pH. Five muscle samples were taken from each treatment group to measure LD and GLY.

Measurement of muscle physical properties

A color-measuring instrument (CR-400, Konica Minolta, Tokyo, Japan) was utilized to assess muscle color according to the procedure of Shi et al.[68]. The shear force was determined using a texture instrument (SD-700, Akiyama Technology Co., Ltd., Dongguan, China) according to the method of Shi et al.[68]. The measurement of muscle WHC was conducted following the method of Peng et al.[14]. Ten muscle samples were taken from each treatment group to measure color and shear force. Five muscle samples were taken from each treatment group to measure WHC.

Measurement of muscle ATP-related compounds

Ultra-high performance liquid chromatography (Acquity UPLC-H Class, Waters Corporation, Milford, MA, USA) was employed to measure the samples, based on the approach of Peng et al.[14]. Six muscle samples were analyzed per treatment group.

Measurement of cortisol, lactate dehydrogenase (LDH), glucose, urea, and creatinine in serum

Serum cortisol levels were evaluated through the use of ELISA kits (Shanghai Jingkang Bioengineering Co., Ltd., Shanghai, China). Lactate dehydrogenase, glucose, urea, and creatinine levels were ascertained with commercial kits (Rayto Life and Analytical Sciences Co., Ltd., Shenzhen, China). Five serum samples were analyzed per treatment group.

Measurement of superoxide dismutase (SOD) and catalase (CAT) in serum and liver

Commercial kits (Nanjing Jiancheng Bioengineering Institute, Nanjing, China) were used to measure superoxide dismutase and catalase levels. Five samples were analyzed for each tissue in each treatment group.

Measurement of the expression of *caspase 3* in the gill and liver

Following sample RNA extraction with TRIzol® Reagent, reverse transcription and real-time quantitative PCR were performed. As the internal reference gene, *β-actin* was applied. Primer sequences were referred to Chen et al.[69] as detailed in Table S1. Assessment of *caspase 3* expression levels was performed with the $2^{-\Delta\Delta CT}$ method. Four samples were analyzed for each tissue in each treatment group.

Observations on the histological structure of the gill, liver, and muscle

Tissues were immersion-fixed in 4% paraformaldehyde for 24 h. Paraffin sectioning of the fixed samples was carried out. After deparaffinization and hematoxylin-eosin staining, the samples were dehydrated and sealed. The treated samples were observed by an optical microscope (Eclipse E100, Nikon, Tokyo, Japan) and scanned by an imaging system (DS-U3, Nikon, Tokyo, Japan). Three samples were analyzed for each tissue in each treatment group.

Muscle transcriptome analysis

RNA was extracted, reverse transcribed, and sequenced as previously described by Chen et al.[70] with slight modifications. Total RNA was isolated from muscle tissue with TRIzol® Reagent. Purify mRNA from total RNA. After that, cDNA was synthesized, and PCR amplification was performed. The library preparations were sequenced with Illumina Novaseq6000 to generate paired-end reads. Then, clean reads were separately compared with the reference genome to obtain the mapping readings. In order to expose the relationship of the samples, principal component analysis (PCA) was used. Differential expression analysis was performed using the DESeq2 (http://bioconductor.org/packages/release/bioc/html/DESeq2.html), genes with $|\log2FC| > 1$ and adjusted p value (Padj) < 0.05 were considered to be significantly differentially expressed genes (DEGs). Heatmap clustering

analysis, GO function enrichment, and KEGG pathway enrichment analysis were performed on DEGs. Six muscle samples were analyzed per treatment group.

To elucidate the key genes affecting muscle quality of silver carp, the WGCNA package was used to perform weighted gene coexpression network analysis of the genes and analyze the correlation between gene modules and muscle quality. Gene-gene interaction networks were mapped for the visualization of gene relationships. Table S1 showed the primer sequences. Analysis of the relative expression levels of DEGs was carried out using the $2^{-\Delta\Delta CT}$ method. Three muscle samples were analyzed per treatment group.

Muscle metabolome analysis

Metabolites were extracted, isolated, characterized, and counted based on the approach of Peng et al.[4] with slight modifications. Using an ultra-high performance liquid chromatograph (1290 infinity LC, Agilent, Palo Alto, California, USA), the samples were separated on an ACQUITY UPLC BEH AMIDE column (1.7 μm, 2.1 × 100 mm, Waters, Milford, USA) for chromatographic separation. A mass spectrometer (AB triple TOF 6600, AB SCIEX, Framingham, USA) was used to analyze the samples. XCMS software served to perform peak alignment, correct retention times, and extract peak areas. The extracted metabolite data underwent multivariate statistical analysis via the website provided by APPLIED PROTEIN TECHNOLOGY on the APT-BioCloud platform (http://www.aptbiotech.com/). Orthogonal Partial Least Squares Discriminant Analysis (OPLS-DA) served to characterize the overall metabolic alterations between groups. Metabolites with a FC > 1.5 or FC < 0.67 and p value < 0.05 were visualized and analyzed as volcano plots. DMs that met VIP > 1 and p value < 0.05 were placed in the KEGG pathway database for pathway enrichment analysis. Six muscle samples were analyzed per treatment group.

Western blotting

The western blotting protocol of Yu et al.[71] was utilized with slight modifications for this study. The primary antibodies used in this study were GAPDH Rabbit mAb (1:5,0000, A19056, ABclonal), Caspase9 rabbit mAb (1:2000, A18676, ABclonal), Caspase8 rabbit mAb (1:2000, A19549, ABclonal), Bax rabbit pAb (1:1000, A0207, ABclonal), and Bcl-2 rabbit mAb (1:2000, A19693, ABclonal). The secondary antibody used in this study was HRP-conjugated Goat anti-Rabbit IgG(H+L) (1:3000, AS014, ABclonal). Three muscle samples were analyzed per treatment group.

Statistical analysis

For biochemical and physical data, the significance of differences among groups was assessed by one-way ANOVA followed by Duncan's multiple comparison test. A p value below 0.05 was deemed indicative of a significant difference. Data from physical measurements were presented as mean ± standard deviation. Graphs were created with GraphPad Prism 8.0 and Origin 2024 software. For the transcriptomic and metabolomic datasets, we used the Benjamini-Hochberg method to perform multiple test corrections on the original p value to control the false discovery rate (FDR). FDR-adjusted p value < 0.05 were deemed significantly altered.

Data availability

All data supporting the findings of this study are available in the paper and Supplementary Information.

Received: 25 June 2025; Accepted: 24 December 2025;
Published online: 07 January 2026

References

1. Fang, D., Mei, J., Xie, J. & Qiu, W. The effects of transport stress (temperature and vibration) on blood biochemical parameters, oxidative stress, and gill histomorphology of pearl gentian groupers. *Fishes* **8**, 218 (2023).
2. Ren, Y. et al. Effects of transportation stress on antioxidation, immunity capacity and hypoxia tolerance of rainbow trout (*Oncorhynchus mykiss*). *Aquac. Rep.* **22**, 100940 (2022).
3. Wang, Q. et al. Transport Stress Induces Oxidative Stress and Immune Response in Juvenile Largemouth Bass (*Micropterus salmoides*): analysis of Oxidative and Immunological Parameters and the Gut Microbiome. *Antioxidants* **12**, 157 (2023).
4. Peng, L. et al. Insight into the mechanism on texture change of Wuchang bream muscle during live transportation using a UPLC-QTOF-MS based metabolomics method. *Food Chem.* **398**, 133796 (2023).
5. Wang, W., Zhang, Y., Liu, Y., Adányi, N. & Zhang, X. Effects of waterless live transportation on survivability, physiological responses and flesh quality in Chinese farmed sturgeon (*Acipenser schrenckii*). *Aquaculture* **518**, 734834 (2020).
6. Wu, Y. et al. Insight into acute heat stress on meat qualities of rainbow trout (*Oncorhynchus mykiss*) during short-time transportation. *Aquaculture* **543**, 737013 (2021).
7. Peng, L. et al. A comprehensive review of the mechanisms on fish stress affecting muscle qualities: nutrition, physical properties, and flavor. *Compr. Rev. Food Sci. Food Saf.* **23**, e13336 (2024).
8. Wu, Y. et al. Effects of hypoxia on meat qualities and muscle metabolism in rainbow trout (Oncorhynchus mykiss) during short-time transportation and its relief by reoxygenation. *Aquaculture* **570**, 739404 (2023).
9. Zhang, T. et al. Recent understanding of stress response on muscle quality of fish: from the perspective of industrial chain. *Trends Food Sci. Technol.* **140**, 104145 (2023).
10. Yuan, L., Jiang, F., Cao, X., Liu, Y. & Xu, Y.-J. Metabolomics reveals the toxicological effects of polar compounds from frying palm oil. *Food Funct.* **11**, 1611–1623 (2020).
11. Li, R. et al. Application of UHPLC-Q-TOF-MS/MS metabolomics approach to investigate the taste and nutrition changes in tilapia fillets treated with different thermal processing methods. *Food Chem.* **356**, 129737 (2021).
12. Wu, Y. et al. Difference in muscle metabolism caused by metabolism disorder of rainbow trout liver exposed to ammonia stress. *Sci. Total Environ.* **924**, 171576 (2024).
13. Shi, G. et al. Integrating transcriptomic and metabolomic analysis to understand muscle qualities of red swamp crayfish (*Procambarus clarkii*) under transport stress. *Food Res. Int.* **164**, 112361 (2023).
14. Peng, L. et al. Effect of respite time before live transportation on muscle quality of blunt snout (Wuchang) Bream. *Foods* **11**, 2254 (2022).
15. Song, L. et al. Effects of saline-alkaline water on growth performance, nutritional processing, and immunity in Nile tilapia (*Oreochromis niloticus*). *Aquaculture* **544**, 737036 (2021).
16. Liu, C., Lin, A., Li, Z., Ma, Z. & Liu, F. Effects of live transport methods on the survivability, physiological responses, and flesh quality of turbot (*Scophthalmus maximus*). *eFood* **5**, e70011 (2024).
17. Cao, J., Wang, Q., Mei, J. & Xie, J. Effect of 3-aminobenzoic acid ethyl ester methanesulfonate (MS-222) on quality of marine cultured turbot *(Scophthalmus maximus*) during simulated transport in water. *Fishes* **6**, 20 (2021).
18. Zhang, Y. et al. Effects of stimulative transportation on the plasma biochemical indices, body color and fillet quality of gibel carp. *Acta Hydrobiol. Sin.* **43**, 86–93 (2019).
19. McKenna, D. R. et al. Biochemical and physical factors affecting discoloration characteristics of 19 bovine muscles. *Meat Sci.* **70**, 665–682 (2005).
20. Zhang, W. et al. Changes in muscle quality of Wuchang Bream during live transportation. *Meat Res.* **36**, 22554 (2022).
21. Refaey, M. M., Tian, X., Tang, R. & Li, D. Changes in physiological responses, muscular composition and flesh quality of channel catfish *Ictalurus punctatus* suffering from transport stress. *Aquaculture* **478**, 9–15 (2017).

22. Chen, Y. et al. The impact of the addition of vitamin C, NaCl, clove oil on the muscle of live blunt-snout bream during transportation. *Food Biosci.* **62**, 105202 (2024).
23. Yu, Q., Liu, J., Hong, H., Gao, R. & Bao, Y. Research progress on the mechanism of water-holding capacity of fresh meat. *Food Sci.* **44**, 241–247 (2023).
24. Gornik, S. G., Albalat, A., Atkinson, R. J. A., Coombs, G. H. & Neil, D. M. The influence of defined ante-mortem stressors on the early post-mortem biochemical processes in the abdominal muscle of the Norway lobster, *Nephrops norvegicus* (Linnaeus, 1758). *Mar. Biol. Res.* **6**, 223–238 (2010).
25. Yang, S. et al. Metabolic responses in *Scophthalmus maximus* kidney subjected to thermal stress. *Fish. Shellfish Immunol.* **103**, 37–46 (2020).
26. Wang, J., Xiong, G., Bai, C. & Liao, T. Anesthetic efficacy of two plant phenolics and the physiological response of juvenile *Ictalurus punctatus* to simulated transport. *Aquaculture* **538**, 736566 (2021).
27. Qiang, J. et al. Water quality and physiological response of F1hybrid seabream (*Pagrus major*♀ × *Acanthopagrus schlegelii*♂) to transport stress at different densities. *Aquac. Res.* **49**, 767–775 (2018).
28. Sintuprom, C. et al. Effects of clove oil concentrations on blood chemistry and stress-related gene expression in Siamese fighting fish (Betta splendens) during transportation. *Front. Vet. Sci.* **11**, 1392413 (2024).
29. Sun, Y., Han, S., Yao, M., Liu, H. & Wang, Y. Exploring the metabolic biomarkers and pathway changes in crucian under carbonate alkalinity exposure using high-throughput metabolomics analysis based on UPLC-ESI-QTOF-MS. *RSC Adv.* **10**, 1552–1571 (2020).
30. Zou, B. et al. Changes of postmortem apoptotic factors, genes and proteins and their potential associations with beef tenderization. *Food Sci. Anim. Prod.* **1**, 9240040–9240040 (2023).
31. Akram, M. Citric acid cycle and role of its intermediates in metabolism. *Cell Biochem. Biophys.* **68**, 475–478 (2013).
32. Wang, T. et al. Metabolic changes and stress damage induced by ammonia exposure in juvenile *Eriocheir sinensis*. *Ecotoxicol. Environ. Saf.* **223**, 112608 (2021).
33. Kang, W., Suzuki, M., Saito, T. & Miyado, K. Emerging role of TCA cycle-related enzymes in human diseases. *Int. J. Mol. Sci.* **22**, 13057 (2021).
34. Wang, Y. et al. Transcriptomic analysis reveals the inhibition mechanism of pulsed light on fungal growth and ochratoxin A biosynthesis in *Aspergillus carbonarius*. *Food Res. Int.* **165**, 112501 (2023).
35. Hsu, H.-P. et al. Mitochondrial phosphoenolpyruvate carboxykinase promotes tumor growth in estrogen receptor-positive breast cancer via regulation of the mTOR pathway. *Cancer Med.* **12**, 1588–1601 (2023).
36. Zeng, S. et al. Role of OGDH in Atophagy-IRF3-IFN-β pathway during classical swine fever virus infection. *Int. J. Biol. Macromol.* **249**, 126443 (2023).
37. Takase, K. & Kakuta, I. Oral administration of wild plant-derived minerals and red ginseng ameliorates insulin resistance in fish through different pathways. *Physiol. Rep.* **11**, e15667 (2023).
38. Wang, Q., Xu, Z. & Ai, Q. Arginine metabolism and its functions in growth, nutrient utilization, and immunonutrition of fish. *Anim. Nutr.* **7**, 716–727 (2021).
39. Liu, N., Zhong, Q., Sun, Z. & Zhang, B. Creatine monohydrate administration delayed muscle glycolysis of antemortem-stressed broilers by enhancing muscle energy status, increasing antioxidant capacity and regulating muscle metabolite profiles. *Poult. Sci.* **104**, 104778 (2025).
40. He, T. et al. Dietary live yeast supplementation alleviates transport-stress-impaired meat quality of broilers through maintaining muscle energy metabolism and antioxidant status. *J. Sci. Food Agric.* **102**, 4086–4096 (2022).
41. Astudillo, A. M., Balboa, M. A. & Balsinde, J. Selectivity of phospholipid hydrolysis by phospholipase A2 enzymes in activated cells leading to polyunsaturated fatty acid mobilization. *Biochim. Biophys. Acta* **1864**, 772–783 (2019).
42. Zheng, Y. et al. Effects of resveratrol on lipid metabolism in liver of red tilapia *Oreochromis niloticus*. *Comp. Biochem. Physiol. Part C Toxicol. Pharmacol.* **261**, 109408 (2022).
43. Kokina, A., Ozolina, Z. & Liepins, J. Purine auxotrophy: possible applications beyond genetic marker. *Yeast* **36**, 649–656 (2019).
44. Wu, L., Pu, H. & Sun, D.-W. Novel techniques for evaluating freshness quality attributes of fish: a review of recent developments. *Trends Food Sci. Technol.* **83**, 259–273 (2019).
45. Jia, R. et al. Chronic exposure of hydrogen peroxide alters redox state, apoptosis and endoplasmic reticulum stress in common carp (*Cyprinus carpio*). *Aquat. Toxicol.* **229**, 105657 (2020).
46. Zheng, X., Xu, D., Sun, L., Qin, X. & Zhang, Y. Inflammation and apoptosis pathways mediated the stress response of Litopenaeus vannamei to acute cold and air exposure during waterless live transportation: based on ultrastructure and transcriptome. *Fish Shellfish Immunol.* **131**, 391–400 (2022).
47. Wang, H. N. et al. Inhibition of c-Fos expression attenuates IgE-mediated mast cell activation and allergic inflammation by counteracting an inhibitory AP1/Egr1/IL-4 axis. *J. Transl. Med.* **19**, 261 (2021).
48. Li, L. et al. Nano-selenium antagonizes heat stress-induced apoptosis of rainbow trout (*Oncorhynchus mykiss*) hepatocytes by activating the PI3K/AKT pathway. *Biol. Trace Elem. Res.* **201**, 5805–5815 (2023).
49. Ji, K. et al. The immunoreaction and antioxidant capacity of juvenile blunt snout bream (*Megalobrama amblycephala*) involves the PI3K/Akt/Nrf2 and NF-κB signal pathways in response to dietary methionine levels. *Fish Shellfish Immunol.* **105**, 126–134 (2020).
50. Jin, X., Hu, Q., Qin, M., Yin, Y. & Xia, Z. Mechanism of Qingre Huatan Tongfu formula in treating ischemic stroke based on network pharmacology. *J. Guangxi Med. Univ.* **41**, 105–112 (2024).
51. Humayun, A. & Fornace, A. J. GADD45 in Stress Signaling, Cell Cycle Control, and Apoptosis in *Gadd45 Stress Sensor Genes* (eds Zaidi, M. R. & Liebermann, D. A.) 1–22 (Springer, Cham, 2022).
52. Ren, Z., Mu, C., Li, R., Song, W. & Wang, C. Characterization of a γ-aminobutyrate type A receptor-associated protein gene, which is involved in the response of *Portunus trituberculatus* to CO_2-induced ocean acidification. *Aquac. Res.* **49**, 2393–2403 (2018).
53. Warner, R. D. et al. Meat tenderness: advances in biology, biochemistry, molecular mechanisms and new technologies. *Meat Sci.* **185**, 108657 (2022).
54. Peng, L. et al. Fasting influences the muscle quality of fish during transportation by regulating the balance between energy metabolism and ammonia nitrogen stress. *J. Adv. Res.* **79**, 75–88 (2026).
55. Chen, J. et al. Pseudo-chromosome-length genome assembly for a deep-sea eel *Ilyophis brunneus* sheds light on the deep-sea adaptation. *Sci. China Life Sci.* **66**, 1379–1391 (2023).
56. Hausrat, T. J., Radwitz, J., Lombino, F. L., Breiden, P. & Kneussel, M. Alpha- and beta-tubulin isotypes are differentially expressed during brain development. *Dev. Neurobiol.* **81**, 333–350 (2021).
57. Randazzo, D. et al. Persistent upregulation of the β-tubulin tubb6, linked to muscle regeneration, is a source of microtubule disorganization in dystrophic muscle. *Hum. Mol. Genet.* **28**, 1117–1135 (2019).
58. Wang, Y. et al. Effects of dietary glutamine supplementation on growth performance, intestinal digestive ability, antioxidant status and hepatic lipid accumulation in *Xenocypris davidi* (Bleeker,1871). *Aquac. Int.* **32**, 725–743 (2024).
59. Zhao, H. F. et al. Flesh shear force, cooking loss, muscle antioxidant status and relative expression of signaling molecules (Nrf2, Keap1, TOR, and CK2) and their target genes in young grass carp

(*Ctenopharyngodon idella*) muscle fed with graded levels of choline. *PLoS ONE* **10**, e0142915 (2015).
60. Ma, X. Z. et al. Enhancement of flavor and healthcare substances, mouthfeel parameters and collagen synthesis in the muscle of on-growing grass carp (*Ctenopharyngodon idella*) fed with graded levels of glutamine. *Aquaculture* **528**, 735486 (2020).
61. Ogun, A. O. et al. Effects of dietary gamma-aminobutyric acid (GABA) inclusion on acute temperature stress responses in juvenile olive flounder (*Paralichthys olivaceus*). *Animals* **15**, 809 (2025).
62. Lu, Y. et al. Cepharanthine, a regulator of keap1-Nrf2, inhibits gastric cancer growth through oxidative stress and energy metabolism pathway. *Cell Death Discov.* **9**, 450 (2023).
63. Choi, G. E. & Han, H. J. Glucocorticoid impairs mitochondrial quality control in neurons. *Neurobiol. Dis.* **152**, 105301 (2021).
64. Yuan, Y. et al. Mechanism of PGC-1α-mediated mitochondrial biogenesis in cerebral ischemia-reperfusion injury. *Front. Mol. Neurosci*. **16**, 1224964 (2023).
65. Mukherjee, A. et al. Mitochondrial reactive oxygen species in infection and immunity. *Biomolecules* **14**, 670 (2024).
66. Dettleff, P. et al. Physiological and molecular responses to thermal stress in red cusk-eel (*Genypterus chilensis*) juveniles reveals atrophy and oxidative damage in skeletal muscle. *J. Therm. Biol.* **94**, 102750 (2020).
67. Xiang, Z. et al. Proteomic analysis revealed the deterioration of surimi gelling capability to fish stress during transportation. *Food Res. Int.* **196**, 115099 (2024).
68. Shi, L. et al. Effect of pre-chilling time on the physicochemical properties of channel catfish during frozen storage. *Int. J. Refrig.* **115**, 56–62 (2020).
69. Chen, S., Xie, L., Yao, C., Li, D. & Tang, R. Role of endoplasmic reticulum stress IRE1 pathway in hepatocyte apoptosis of grass carp *ctenopharyngodon idella* induced by sodium nitrite. *Acta Hydrobiol. Sin.* **44**, 10–19 (2020).
70. Chen, Y. et al. Integrated metabolomic and transcriptomic responses to heat stress in a high-altitude fish, *Triplophysa siluroides*. *Fish. Shellfish Immunol.* **142**, 109118 (2023).
71. Yu, H. et al. Comprehensive analysis of transcriptome and metabolome reveals regulatory mechanism of intramuscular fat content in beef cattle. *J. Agric. Food Chem.* **72**, 2911–2924 (2024).

Acknowledgements

The authors gratefully acknowledge financial support from the earmarked fund for CAR (CARS-45).

Author contributions

Yujie Meng: writing—original draft, methodology, investigation, formal analysis, data curation. Liangzi Zhang: Writing—review and editing, validation. Shikang Sang: methodology, formal analysis. Zenan Huang: writing—review and editing. Ru Liu: funding acquisition. Juan You: validation. Qilin Huang: supervision. Yong Long: investigation. Guili Song: investigation. Dan Jia: validation. Tao Yin: writing—review and editing, methodology, conceptualization.

Competing interests

The authors declare no competing interests.

Additional information

Supplementary information The online version contains supplementary material available at https://doi.org/10.1038/s41538-025-00691-6.

Correspondence and requests for materials should be addressed to Dan Jia or Tao Yin.

Reprints and permissions information is available at http://www.nature.com/reprints

Publisher's note Springer Nature remains neutral with regard to jurisdictional claims in published maps and institutional affiliations.

Open Access This article is licensed under a Creative Commons Attribution-NonCommercial-NoDerivatives 4.0 International License, which permits any non-commercial use, sharing, distribution and reproduction in any medium or format, as long as you give appropriate credit to the original author(s) and the source, provide a link to the Creative Commons licence, and indicate if you modified the licensed material. You do not have permission under this licence to share adapted material derived from this article or parts of it. The images or other third party material in this article are included in the article's Creative Commons licence, unless indicated otherwise in a credit line to the material. If material is not included in the article's Creative Commons licence and your intended use is not permitted by statutory regulation or exceeds the permitted use, you will need to obtain permission directly from the copyright holder. To view a copy of this licence, visit http://creativecommons.org/licenses/by-nc-nd/4.0/.

© The Author(s) 2026